half-time of 0.25 ms. The maximum excitatory conductance was $G_{E,max} = 1.5$ nS. All 2×24 excitatory and 24 inhibitory pre-synaptic inputs were generated independently by an auditory nerve model[30] that produced about 160 spikes in response to the 1-s-tone-burst stimulus when the tone's frequency equals the best frequency. The contralateral inhibition led the excitation from either side by 0.2 ms. For simplicity, the simulations of cochlear nucleus neurons and inhibitory interneurons in the trapezoid body were omitted.

Received 31 December 2001; accepted 13 March 2002.

1. Jeffress, L. A. A place theory of sound localization. *J. Comp. Physiol. Psychol.* **41,** 35–39 (1948).
2. Joris, P. X., Smith, P. H. & Yin, T. C. Coincidence detection in the auditory system: 50 years after Jeffress. *Neuron* **21,** 1235–1238 (1988).
3. Grothe, B. & Sanes, D. H. Synaptic inhibition influences the temporal coding properties of medial superior olivary neurons: an in vitro study. *J. Neurosci.* **14,** 1701–1709 (1994).
4. Klumpp, R. & Eady, H. Some measurements of interaural time difference thresholds. *J. Acoust. Soc. Am.* **28,** 215–232 (1956).
5. Overholt, E., Rubel, E. W. & Hyson, R. L. A circuit for coding interaural time differences in the chick brainstem. *J. Neurosci.* **12,** 1698–1708 (1992).
6. Carr, C. E. & Konishi, M. Axonal delay lines for time measurement in the owl's brainstem. *Proc. Natl Acad. Sci. USA* **85,** 8311–8315 (1988).
7. Smith, P. H., Joris, P. X. & Yin, T. C. Projections of physiologically characterized spherical bushy cell axons from the cochlear nucleus of the cat: evidence for delay lines to the medial superior olive. *J. Comp. Neurol.* **331,** 245–260 (1993).
8. Grothe, B. The evolution of temporal processing in the medial superior olive, an auditory brainstem structure. *Prog. Neurobiol.* **61,** 581–610 (2000).
9. Yin, T. C. & Chan, J. C. Interaural time sensitivity in medial superior olive of cat. *J. Neurophys.* **64,** 465–488 (1990).
10. Spitzer, M. W. & Semple, M. N. Neurons sensitive to interaural phase disparity in gerbil superior olive: diverse monaural and temporal response properties. *J. Neurophys.* **73,** 1668–1690 (1995).
11. Cant, N. B. & Hyson, R. L. Projections from the lateral nucleus of the trapezoid body to the medial superior olivary nucleus in the gerbil. *Hearing Res.* **58,** 26–34 (1992).
12. Kuwabara, N. & Zook, J. M. Projections to the medial superior olive from the medial and lateral nuclei of the trapezoid body in rodents and bats. *J. Comp. Neurol.* **324,** 522–538 (1992).
13. Grothe, B. & Sanes, D. H. Bilateral inhibition by glycinergic afferents in the medial superior olive. *J. Neurophys.* **69,** 1192–1196 (1993).
14. Smith, A. J., Owens, S. & Forsythe, I. D. Characterisation of inhibitory and excitatory postsynaptic currents of the rat medial superior olive. *J. Physiol.* **529,** 681–698 (2000).
15. Grothe, B. & Park, T. J. Sensitivity to interaural time differences in the medial superior olive of a small mammal, the Mexican free-tailed bat. *J. Neurosci.* **18,** 6608–6622 (1998).
16. Heffner, R. S. & Heffner, H. E. Sound localization and use of binaural cues by the gerbil (*Meriones unguiculatus*). *Behav. Neurosci.* **102,** 422–428 (1988).
17. McAlpine, D., Jiang, D. & Palmer, A. R. A neural code for low-frequency sound localization in mammals. *Nature Neurosci.* **4,** 396–401 (2001).
18. Grothe, B., Park, T. J. & Schuller, G. Medial superior olive in the free-tailed bat: response to pure tones and amplitude-modulated tones. *J. Neurophys.* **77,** 1553–1565 (1997).
19. Rothman, J. S., Young, E. D. & Manis, P. B. Convergence of auditory nerve fibers onto bushy cells in the ventral cochlear nucleus: implications of a computational model. *J. Neurophys.* **70,** 2562–2583 (1993).
20. Smith, P. H., Joris, P. X. & Yin, T. C. Anatomy and physiology of principal cells of the medial nucleus of the trapezoid body (MNTB) of the cat. *J. Neurophys.* **79,** 3127–3142 (1998).
21. Taschenberger, H. & von Gersdorff, H. Fine-tuning an auditory synapse for speed and fidelity: developmental changes in presynaptic waveform, EPSC kinetics, and synaptic plasticity. *J. Neurosci.* **20,** 9162–9173 (2000).
22. Grothe, B. Interaction of excitation and inhibition in processing of pure tone and amplitude-modulated stimuli in the medial superior olive of the mustached bat. *J. Neurophys.* **71,** 706–721 (1994).
23. Kapfer, C., Seidl, A. H., Schweizer, H. & Grothe, B. Experience-dependent refinement of inhibitory inputs to auditory coincidence-detector neurons. *Nature Neurosci.* **5,** 257–253 (2002).
24. Willott, J. F., Milbrandt, J. C., Bross, L. S. & Caspary, D. M. Glycine immunoreactivity and receptor binding in the cochlear nucleus of c57bl/6j and cba/caj mice: effects of cochlear impairment and aging. *J. Comp. Neurol.* **385,** 405–414 (1997).
25. Goldberg, J. M. & Brown, P. B. Response of binaural neurons of dog superior olivary complex to dichotic tonal stimuli: some physiological mechanisms of sound localization. *J. Neurophys.* **32,** 613–636 (1969).
26. Havey, D. C. & Caspary, D. M. A simple technique for constructing 'piggy-back' multibarrel microelectrodes. *Electroencephalogr. Clin. Neurophys.* **48,** 249–251 (1980).
27. Brand, A., Urban, A. & Grothe, B. Duration tuning in the mouse auditory midbrain. *J. Neurophys.* **84,** 1790–1799 (2000).
28. Yin, T. C. & Kuwada, S. Binaural interaction in low-frequency neurons in inferior colliculus of the cat. III. Effects of changing frequency. *J. Neurophys.* **50,** 1020–1042 (1983).
29. Brughera, A. R., Stutman, E. R., Carney, L. H. & Colburn, H. S. A model with exitation and inhibition for cells in the medial superior olive. *Audit. Neurosci.* **2,** 219–233 (1996).
30. Carney, L. H. A model for the responses of low-frequency auditory-nerve fibers in cat. *J. Acoust. Soc. Am.* **93,** 401–417 (1993).

Acknowledgements

We thank G. Breutel for technical assistance, C. Kapfer for suggestions, and M. Goetz for critical comments on the manuscript. This work was supported by the German Research Foundation (A.B., O.B., B.G.) and by the Medical Research Council (T.M., D.M.).

Competing interests statement

The authors declare that they have no competing financial interests.

Correspondence and requests for materials should be addressed to B.G. (e-mail: bgrothe@neuro.mpg.de).

Nogo-66 receptor antagonist peptide promotes axonal regeneration

Tadzia GrandPré*, Shuxin Li* & Stephen M. Strittmatter

Department of Neurology and Section of Neurobiology, Yale University School of Medicine, P.O. Box 208018, New Haven, Connecticut 06520, USA
** These authors contributed equally to this work*

Myelin-derived axon outgrowth inhibitors, such as Nogo, may account for the lack of axonal regeneration in the central nervous system (CNS) after trauma in adult mammals. A 66-residue domain of Nogo (Nogo-66) is expressed on the surface of oligodendrocytes[1] and can inhibit axonal outgrowth through an axonal Nogo-66 receptor (NgR)[2]. The IN-1 monoclonal antibody recognizes Nogo-A and promotes corticospinal tract regeneration and locomotor recovery[3–5]; however, the undefined nature of the IN-1 epitope in Nogo, the limited specificity of IN-1 for Nogo, and nonspecific anti-myelin effects have prevented a firm conclusion about the role of Nogo-66 or NgR. Here, we identify competitive antagonists of NgR derived from amino-terminal peptide fragments of Nogo-66. The Nogo-66(1–40) antagonist peptide (NEP1–40) blocks Nogo-66 or CNS myelin inhibition of axonal outgrowth *in vitro*, demonstrating that NgR mediates a significant portion of axonal outgrowth inhibition by myelin. Intrathecal administration of NEP1–40 to rats with mid-thoracic spinal cord hemisection results in significant axon growth of the corticospinal tract, and improves functional recovery. Thus, Nogo-66 and NgR have central roles in limiting axonal regeneration after CNS injury, and NEP1-40 provides a potential therapeutic agent.

Previously, we sought to determine which residues within the Nogo-66 domain are responsible for inhibition of axon outgrowth[1]. Five 25-residue peptides, consisting of overlapping segments of the Nogo-66 sequence, were assessed in axonal outgrowth assays. Only the peptide consisting of residues 31–55 is inhibitory, demonstrating the role of these residues in receptor activation. However, the inhibitory potency of this peptide is three orders of magnitude less than the entire 66-residue fragment, suggesting that regions other than residues 31–55 contribute to high-affinity binding of Nogo-66 to its receptor. To determine which Nogo-66 residues are required for high-affinity binding, we produced fusion proteins of placental alkaline phosphatase (AP) and various fragments of Nogo-66. Several of the Nogo-66 deletion mutants bind as avidly as Nogo-66 to COS7 cells expressing NgR (Fig. 1a). Notably, the deletion of residues 34–66, encompassing half of the Nogo-66 sequence, does not prevent high-affinity binding by the Nogo-66(1–33) fusion protein. Binding of the Nogo-66(1–31) fusion protein is slightly reduced (dissociation constant, $K_d = 24 \pm 11$ nM; Fig. 1a and data not shown) compared with the Nogo-66(1–33) and longer fusion proteins (K_d values $= 11–14 \pm 3$ nM). Additional deletions from the carboxyl end of Nogo-66 markedly reduce NgR binding, such that proteins containing fewer than the 31 N-terminal residues of Nogo-66 exhibit no binding to NgR under these conditions. The necessity of residues at the N terminus was tested in the setting of the Nogo-66(1–40) fusion protein. Deletion of five N-terminal residues in the Nogo-66(6–40) protein significantly reduces binding, and deletion of ten residues (Nogo-66(11–40) protein) abolishes binding. Thus, residues 1–31 seem to be sufficient for high-affinity binding to NgR. Within the N-terminal portion of Nogo-66, at least some of the first ten residues (RIYKGVIQA) and residues in the 30–33 region (SEEL) are necessary for maximal binding. The necessity of specific residues from 11–30 for high-affinity binding is not tested here.

As the minimal high-affinity binding domain has little overlap with the 31–55-residue peptide, which exhibits weak agonist activity, we considered the possibility that the N-terminal segment of Nogo-66 might bind to, but not activate, NgR in neurons. Although the full AP–Nogo-66 domain is a potent growth-cone-collapsing agent, the truncated AP–Nogo fusion proteins do not induce growth-cone collapse in embryonic day 12 (E12) chick dorsal root ganglion (DRG) explant cultures (Fig. 1b). Thus, high-affinity binding to NgR can be dissociated from activation of an inhibitory signal through NgR.

The characteristics of the C-terminal-deleted Nogo-66 derivatives suggest that they might function competitively as NgR antagonists. A synthetic Nogo-66(1–40) peptide (Nogo extracellular peptide, residues 1–40, NEP1–40) does not collapse E12 chick DRG growth cones, even at 1 μM concentrations, consistent with the fusion protein results (Fig. 1d, e). To test for receptor antagonist activity, NEP1–40 was added to E12 chick DRG explant cultures in conjunction with the NgR agonists glutathione *S*-transferase (GST)–Nogo-66 and AP–Nogo-66. NEP1–40 blocks both AP–Nogo-66 binding (Fig. 1c) and GST–Nogo-66-induced growth-cone collapse (Fig. 1d), as expected for a competitive NgR antagonist. This effect is specific for NgR in that growth-cone collapse by semaphorin 3A (Sema3A) and phorbol ester are not altered by NEP1–40 (Fig. 1e and data not shown). We also assessed the ability of NEP1–40 to neutralize Nogo-66-induced inhibition of neurite outgrowth (Fig. 1f). Soluble NEP1–40 alone has no observable effect on neurite outgrowth from these cells, but it reverses the inhibitory effect of bound GST–Nogo-66. A scrambled sequence version of NEP1–40 does not possess NgR antagonist activity. A second domain of Nogo-A, Amino-Nogo, seems to inhibit outgrowth by a mechanism independent of NgR[2,6], and is not blocked by NEP1–40 (Fig. 1f). Taken together, these studies demonstrate that NEP1–40 is a potent NgR competitive antagonist *in vitro*.

The identification of NEP1–40 as a selective NgR antagonist allows an assessment of the relative contribution of NgR ligands to the inhibitory quality of CNS myelin on axon outgrowth. When applied to E12 chick DRG explant cultures, purified CNS myelin potently collapses growth cones and inhibits axonal extension. The presence of NEP1–40 attenuates outgrowth inhibition by CNS myelin, demonstrating that NgR is a significant mediator of inhibition under these conditions (Fig. 2). The potency of NEP1–40 in reversing myelin inhibition is characterized by an effector concentration for half-maximum response (EC_{50}) of 50 nM peptide (Fig. 2b), quite similar to the K_d of AP–Nogo-66(1–40) for NgR (Fig. 1). Myelin inhibition of axon growth is not completely blocked by NEP1–40 even at high peptide concentrations (Fig. 2c). This NEP1–40-insensitive axon outgrowth inhibition by CNS myelin is probably attributable to molecules other than Nogo-66, such as

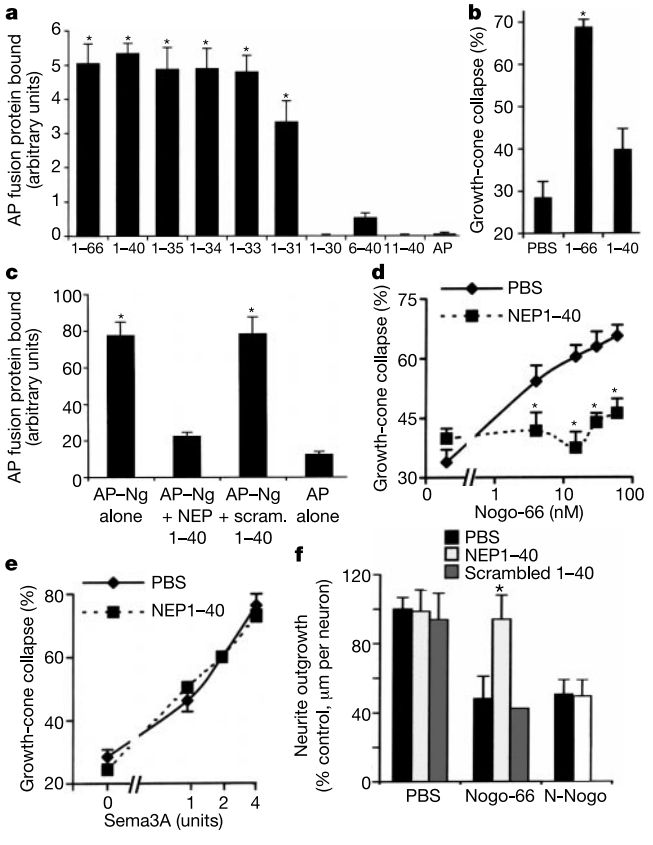

Figure 1 NEP1–40 is a competitive antagonist of Nogo-66. **a**, Conditioned medium containing the indicated Nogo-66-derived AP fusion proteins (28 nM) was applied to COS7 cells expressing NgR. **b**, E12 chick DRG growth-cone morphology after a 30-min exposure to 20 nM AP fusion protein. **c**, Binding of 5 nM AP–Nogo-66 or 5 nM AP to E13 chick DRG axons quantified in the presence or absence of 1 μM NEP1–40 or scrambled NEP1–40. Ng, Nogo. **d**, **e**, Growth-cone collapse measured in cultures pre-treated with either 1 μM NEP1–40 or buffer before a 30-min exposure to various concentrations of GST–Nogo-66 (**d**), or Sema3A (**e**). **f**, Neurite outgrowth is reported for dissociated E12 chick DRG neurons grown for 5–7 h on bound substrate coating (GST–Nogo-66 (7.5 ng), Amino-Nogo (N-Nogo; 7.5 ng) or PBS) after treatment with 1 μM NEP1–40, a scrambled version of NEP1–40, or buffer. Data are the means + s.e.m. from 5–6 determinations. Those values statistically different from control are indicated with an asterisk ($P < 0.05$, Student's *t*-test).

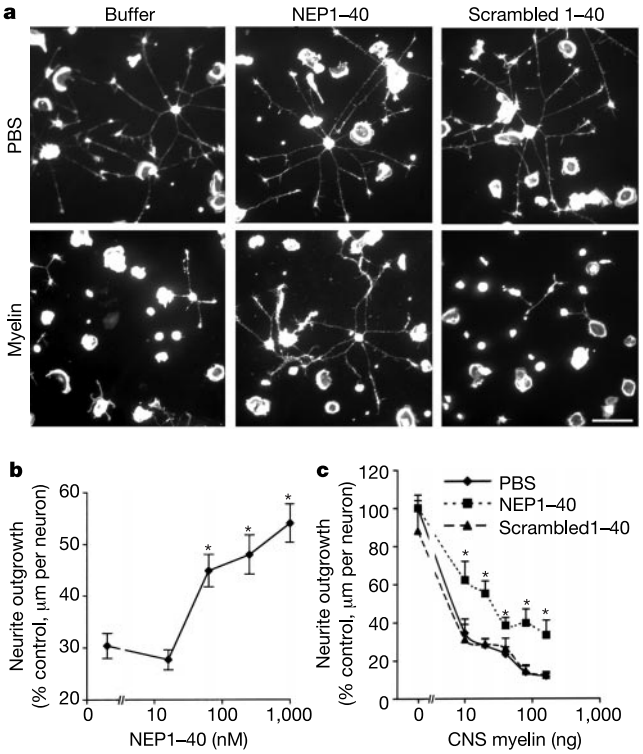

Figure 2 NEP1–40 partially blocks inhibitory activity of CNS myelin. **a**, Dissociated E12 chick DRG cultures grown on a bound substrate coating (CNS myelin or PBS) with 1 μM soluble NEP1–40, a scrambled version of NEP1–40, or buffer. Scale bar, 75 μm. **b**, E12 chick DRG neurons were cultured on a substrate coated with 20 ng myelin protein per 3-μl spot in the presence of the indicated concentrations of NEP1–40. Outgrowth in the absence of CNS myelin is 100%. **c**, Neurite outgrowth from E12 chick dissociated DRGs as in **a** was measured. Cultures were grown 5–7 h on a bound substrate coating (CNS myelin or PBS) with soluble NEP1–40, scrambled NEP1–40, or buffer. Means + s.e.m. from 4–9 experiments are reported. The NEP1–40 values are statistically different from the corresponding control (asterisk, $P < 0.05$, Student's *t*-test).

Amino-Nogo (Fig. 1)[2], myelin-associated glyroprotein (MAG)[7,8] or chondroitin sulphate proteoglycans[9].

To the extent that NgR is responsible for limiting axonal regeneration *in vivo* after trauma, NgR antagonism by the NEP1–40 peptide should stimulate regeneration after CNS injury. We delivered the peptide or vehicle intrathecally to rats at the site of a mid-thoracic dorsal hemisection injury through an osmotic minipump. A dose of 75 μg NEP1–40 per kg body weight per day was administered for four weeks in this protocol. The integrity of the descending corticospinal tract (CST) was traced by injection of biotin dextran amine (BDA) into the motor cortex. In rats receiving the vehicle control, the prominent dorsal CST (DCST) is tightly bundled above the lesion site (Fig. 3) and stops abruptly at the transection site. Fewer fibres are observed in the ventral CST (VCST) and only a few dorsolateral CST fibres are detectable (Fig. 3a–c). This pattern is consistent with published reports[10]. Below the level of the lesion, a small number of fibres are present but these are confined to the position of the uninjured VCST (Fig. 4e–g).

Samples from injured rats treated with NEP1–40 exhibit an entirely different pattern of labelling. Rostral to the lesion, numerous ectopic fibres sprouting from the labelled CST are observed (Fig. 3b, c). In some cases, projections cross from the DCST near the midline to the circumference of the cord, becoming intermingled with the dorsolateral CST. The sprouting axons extend through grey matter to a greater extent than white matter. A measure of ectopic sprouting adjacent to the DCST reveals a greater than tenfold increase in the peptide-treated animals (Fig. 3b, c). Multiple fibres of this type were seen in every injured animal that had been treated with the peptide. This cannot be attributed to different degrees of BDA uptake, as the total number of fibres in the dorsal and ventral CSTs above the lesion is indistinguishable between peptide and control sections (Fig. 3a). The sprouting response is due to a combination of NEP1–40 plus axotomy, as no such change is observed in the CST of uninjured rats treated with intrathecal NEP1–40 (Fig. 3b). Similarly, no collateral sprouts from the uninjured VCST of hemisected rats treated with NEP1–40 are observed rostral to the lesion (data not shown).

Longitudinal sections across the lesion site in both groups of rats reveal scarring and cavity formation extending from the dorsal surface to, or slightly beyond, the central canal (Fig. 3d–f). The linear projection of the DCST ends at or immediately above the injury site in all animals. In sections from the control group of animals, only occasional fibres in the VCST extend rostral to caudal in a linear fashion, consistent with the labelling of the uninjured VCST. In the NEP1–40 group, a plexus of convoluted fibres crosses from the rostral to caudal cord primarily within the ventral half of the cord (Fig. 3e, f).

Multiple ectopic CST fibres are present throughout the grey and white matter of the lower thoracic spinal cord of the NEP1–40-treated rats (Fig. 4b, d). Even at distances of 11–15 mm caudal to the lesion site, 20–30 CST fibres are observed in each section from these animals, as compared with 0–2 fibres in vehicle-treated rats (Fig. 4e, f). Most of these fibres do not possess the linear trajectory of uninjured fibres but follow branching and tortuous courses. A significant fraction of the fibres are located in the dorsal half of the cord, and some are present in the white matter of the dorsal

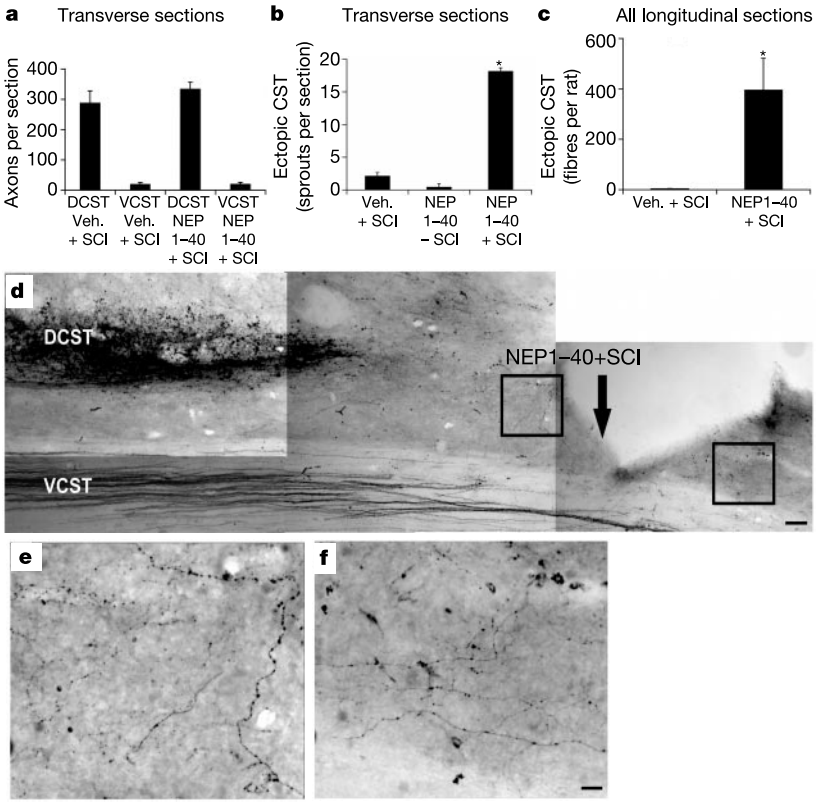

Figure 3 NEP1–40 promotes dorsal CST sprouting rostral to mid-thoracic dorsal hemisection. **a**, Number of BDA-labelled fibres within the DCST or VCST from vehicle (Veh.) and NEP1–40-treated rats in transverse sections 11–15 mm above the lesion. **b**, Number of BDA-labelled fibres outside of the DCST and longer than 200 μm in the transverse plane from transverse sections. **c**, The total number of ectopic fibres in all consecutive saggital sections lateral to the DCST and 1–10 mm rostral to the lesion site. Only those fibres with a dorsoventral projection of at least 200 μm are scored in order to exclude longitudinally projecting fibres. SCI, spinal cord injury. **d**, Parasaggital section containing the site of the transection (arrow) from a NEP1–40-treated rat demonstrates numerous labelled fibres in the DCST ending at the injury site. Numerous branched, sprouting fibres are seen in the ventral half of the cord in the two boxed areas. Higher magnification views of these areas in **e** (left box) and **f** (right box) illustrate the meandering course of the regenerating fibres in the NEP1–40-treated rats. A few VCST fibres are seen in the lower half of the figure. Scale bar, 100 μm (**d**); 25 μm (**e**, **f**). Means + s.e.m. from six rats in each group are reported. The NEP1–40 values are statistically different from control (asterisk, $P < 0.05$, Student's *t*-test).

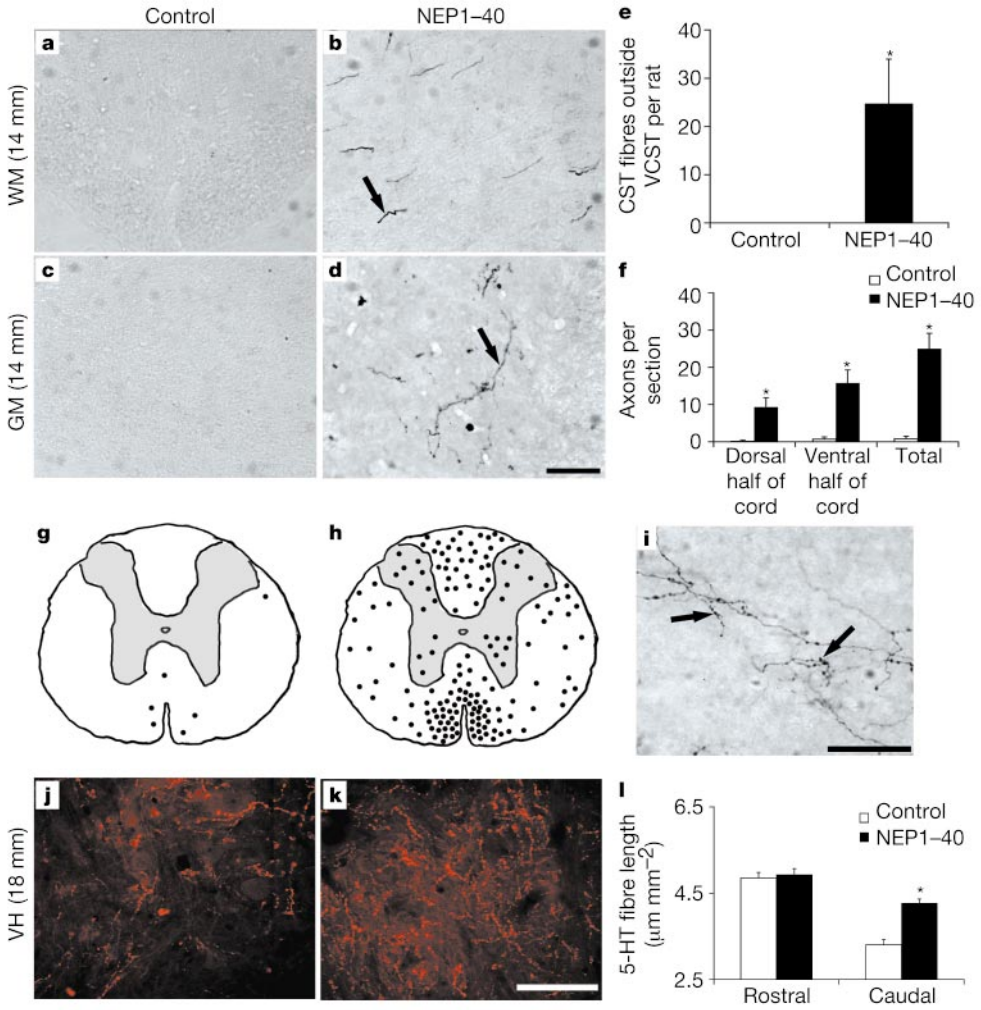

Figure 4 Numerous regenerating CST fibres caudal to a mid-thoracic dorsal hemisection. **a**–**d**, Transverse sections of dorsal white matter (WM; **a**, **b**) or dorsal grey matter (GM; **c**, **d**) at a level 14 mm caudal to the hemisection reveal no CST fibres in sections from vehicle-treated animals (**a**, **c**), but numerous CST axons (arrows) in the peptide-treated animals (**b**, **d**). **e**, Number of fibres outside of the ventral CST in all consecutive saggital sections from the tissue of single rats at a level 1–10 mm caudal to the lesion site. **f**, Number of BDA-labelled fibres per section, as in **a**–**d**, measured in transverse sections 11–15 mm caudal to the lesion. Means + s.e.m. from six rats in each group are reported. **g**, **h**, Locations of labelled fibres in transverse sections at a level 11–15 mm below the lesion site illustrated as a dot for one section from each of five rats (vehicle, **g**; NEP1–40, **h**). The diagram reflects the total number of fibres from five rats. **i**, CST fibres in the ventral horn of an injured rat treated with NEP1–40 exhibit specializations (arrows) consistent with synaptic boutons. **j**, **k**, Serotonin immunoreactivity in the ventral horn (VH) 18 mm below the dorsal hemisection is greater for NEP1–40-treated rats (**k**) than for vehicle-treated animals (**j**). **l**, Serotonin fibre density in the ventral horn was measured 20 mm rostral or 20 mm caudal to a hemisection in control or NEP1–40-treated rats. Scale bars, 25 μm. Means + s.e.m. from six rats in each group are reported. Where indicated, the NEP1–40 values are statistically different from control (asterisk, $P < 0.01$, Student's *t*-test).

column, the site of the injured DCST (Fig. 4h). Several factors make it unlikely that collateral sprouting from uninjured VCST fibres accounts for a significant fraction of the caudal CST fibres in rats with spinal-cord injury treated with NEP1–40. NEP1–40 does not induce collateral sprouting from the DCST in the upper thoracic cord of uninjured rats (Fig. 3b) or the upper thoracic VCST of injured rats. The number of fibres in any one section (approximately 25, Fig. 4e, f) is much greater than the average number in the control VCST caudal to the lesion (about 1, Fig. 4f). Therefore, the numerous regenerating CST fibres in the spinal cord caudal to the injury probably derive from long-distance growth of the numerous ectopic DCST sprouts identified above the lesion site. High magnification views of CST fibres in the lower thoracic ventral horn of rats with spinal cord injury treated with NEP1–40 demonstrate morphology consistent with synaptic boutons, suggesting that functional connections are formed by these regenerating fibres (Fig. 4i).

The dorsal hemisection severs a fraction of serotonin-containing raphespinal fibres. Four weeks after injury, the lower thoracic ventral horn of control rats exhibits a 40% reduction in the density of 5-hydroxytryptamine (5-HT)-positive fibres compared with sections rostral to the spinal cord injury (Fig. 4j–l). In samples from injured rats treated with NEP1–40, the density of 5-HT-positive fibres from the lower thoracic ventral horn is nearly identical to control values in rostral sections. Thus, NEP1–40 treatment promotes the regeneration of both corticospinal and raphespinal axons. The regeneration of 5-HT fibre density may be due to a combination of collateral sprouting in the caudal spinal cord and long distance axonal growth from severed serotonin-containing axons.

A standardized BBB locomotor score[11] (0–21, with 21 being normal function) was used to assess the degree of functional recovery after dorsal hemisection of the spinal cord with or without NEP1–40 treatment (Fig. 5). Those animals receiving NEP1–40 have significantly higher BBB scores by 14 days after spinal cord injury, and this improvement with NEP1–40 persists through 28 days. At the time points of two and seven days, but not at the 4-h time point, there is a lesser degree of improvement in the NEP1–40 group.

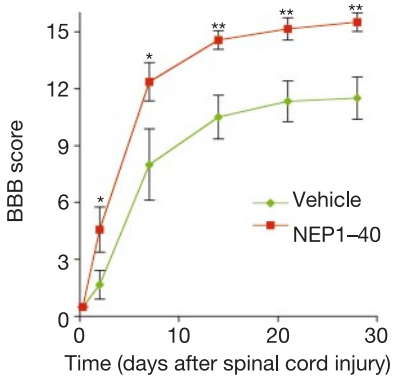

Figure 5 NEP1–40 promotes locomotor recovery after spinal cord injury. The BBB score was determined at the indicated times after mid-thoracic dorsal hemisection in vehicle-treated or NEP1–40-treated rats. The first time point is 4 h after injury when the effects of anaesthetic are nil. Mean + s.e.m. from 6 or 7 rats in each group. Where indicated, the NEP1–40 values are statistically different from control for each day (asterisk, $P < 0.05$; double asterisk, $P < 0.01$, Student's *t*-test).

It may be that functional improvements in the first several days relate to increased collateral sprouting from uninjured axons in the caudal spinal cord, whereas the more significant improvements at later times are dependent on long-distance axonal growth from severed axons.

The principal findings of this study are the identification of a NgR antagonist peptide and the demonstration that a selective NgR antagonist promotes axonal regeneration in rats with spinal cord injury. These data establish a role for Nogo-66 and NgR in limiting axonal regeneration *in vivo*. Analysis of ligand binding to the NgR reveals that a high-affinity binding domain is largely separable from the amino acid residues involved in activating NgR signalling in neurons. As the NEP1–40 peptide is a competitive antagonist of the NgR, its ability to attenuate CNS myelin inhibition of axonal growth demonstrates that the NgR mediates a significant fraction of this inhibition. Local administration of the NgR antagonist peptide to animals after mid-thoracic dorsal spinal cord hemisection elicits a clear axon sprouting response and significant functional recovery. The number of CST fibres at a location over 1 cm caudal to the lesion is about 10% of the total labelled fibres above the lesion. The high potency, selectivity and efficacy of NEP1–40 raises the possibility that a NgR antagonist might be an effective therapeutic agent in clinical conditions characterized by a failure of axonal regeneration, including spinal cord injury, brain trauma, white matter stroke and chronic progressive multiple sclerosis. □

Methods

Nogo-66-derived AP fusion proteins and NEP1–40 synthesis

To generate AP fusion proteins, the relevant regions of human Nogo-A complementary DNA were amplified by polymerase chain reaction and ligated into the pcAP-6 vector as described for AP–Nogo-66 (ref. 2). Binding of AP–Nogo fusion proteins to COS7 cells expressing wild-type NgR and to chick E12 DRG neurons has been described[2]. The NEP1–40 peptide (acetyl-RIYKGVIQAIQKSDEGHPFRAYLESEVAISEELVQKYSNS-amide) was synthesized using tBOC chemistry at the W. M. Keck Biotechnology Center of Yale University. After preparative reverse phase high-performance liquid chromatography purification, a purity greater than 98% was verified by electrospray ionization spray mass spectrometry. Preparation of GST–Nogo-66 (ref. 1), AP–Nogo-66 (ref. 2), Amino-Nogo[2], Sema3A (ref. 12) and CNS myelin[13] were as described.

Growth-cone collapse and neurite outgrowth

E12 chick DRG growth-cone collapse and neurite outgrowth assays have been described[1]. For antagonism assays of growth-cone collapse, NEP1–40 was added 10 min before collapsing agent. For assays of neurite outgrowth, plastic chamber slides were coated with 100 $\mu g\,ml^{-1}$ poly-L-lysine, washed, and dried. Three-microlitre drops of PBS containing GST–Nogo-66, Amino-Nogo or CNS myelin were spotted and dried. Slides were then rinsed and coated with 10 $\mu g\,ml^{-1}$ laminin before addition of dissociated E12 chick DRGs. We added NEP1–40, or a scrambled version of NEP1–40, at the time of cell plating. We incubated cultures for 5–7 h before assessing neurite outgrowth.

Spinal cord transection and axonal tracing

Female Sprague–Dawley rats (175–250 g) were deeply anaesthetized with ketamine (60 mg per kg) and xylazine (10 mg per kg). Laminectomy was conducted at spinal levels of T6 and T7, and the spinal cord was exposed. The dorsal half of the spinal cord was cut with a pair of microscissors to sever the dorsal parts of the corticospinal tracts, and the depth of lesion (approximately 1.8 mm) was assured by passing the sharp part of a number 11 blade across the dorsal half of the cord. An osmotic minipump (Alzet 2004, ~240 µl volume, 0.30 $\mu l\,h^{-1}$, 28 day delivery), which was filled with 97.5% PBS plus 2.5% DMSO or 500 µM NEP1–40 in 97.5% PBS plus 2.5% DMSO, was sutured to muscles under the skin on the back of the animals. A catheter connected to the outlet of the minipump was inserted into the intrathecal space of the spinal cord at the T7 level through a small hole in the dura. For those rats receiving NEP1–40 without spinal cord injury, the laminectomy and minipump placement were accomplished in the same fashion. Two weeks after lesion, a burr hole was made on each side of the skull overlying the sensorimotor cortex of the lower limbs. The anterograde neuronal tracer biotin dextran amine (BDA, 10% in PBS, 3.5 µl per cortex) was applied at seven injection sites at a depth of 1.5 mm from the cortical surface on each side. Two weeks after BDA injection, the animals were killed by perfusion with PBS, followed by 4% paraformadehyde. The spinal cord extending from 10 mm rostral to 10 mm caudal from the lesion site was cut parasaggitally (50 µm) on a vibrating microtome. Transverse sections were collected from the spinal cord 11–16 mm rostral to and 11–16 mm caudal to the injury site. The sections were incubated with avidin-biotin-peroxidase complex and the BDA tracer was visualized by nickel-enhanced diaminobenzidine HRP reaction[14]. Some sections were processed for serotonin immunohistochemistry (anti-5-HT antibody; Instar) by indirect immunofluoresence. We processed confocal images using NIH Image software.

Throughout the surgery, post-operative care, behavioural observation and histological analysis, researchers were blind to the identity of the compound in the minipump. A total of 50 rats underwent the full procedure, 23 receiving vehicle and 27 receiving NEP1–40. During the first nine days after spinal cord injury, 30% of the control group and 33% of the NEP1–40 group died or were killed owing to poor general health. Thus, 16 control and 18 NEP1–40-treated animals completed the study. One rat was excluded from the anatomical analysis owing to an incomplete lesion documented by numerous uninjured dorsal CST fibres at four weeks, and a lack of disability (BBB score of 14) at two days after injury. For axon counts, sections from the first six rats processed were scored for each treatment group. In axon counts, a cluster of branched and connected fibres was counted as one; only labelled fibres separated by more than 50 µm were counted separately. For behavioural analysis, six vehicle-treated and seven NEP1–40-treated rats were compared using the BBB scale[11].

Received 26 January; accepted 25 March 2002.

1. GrandPre, T., Nakamura, F., Vartanian, T. & Strittmatter, S. M. Identification of the Nogo inhibitor of axon regeneration as a Reticulon protein. *Nature* **403,** 439–444 (2000).
2. Fournier, A. E., GrandPre, T. & Strittmatter, S. M. Identification of a receptor mediating Nogo-66 inhibition of axonal regeneration. *Nature* **409,** 341–346 (2001).
3. Chen, M. S. *et al.* Nogo-A is a myelin-associated neurite outgrowth inhibitor and an antigen for monoclonal antibody IN-1. *Nature* **403,** 434–439 (2000).
4. Bregman, B. S. *et al.* Recovery from spinal cord injury mediated by antibodies to neurite growth inhibitors. *Nature* **378,** 498–501 (1995).
5. Merkler, D. *et al.* Locomotor recovery in spinal cord-injured rats treated with an antibody neutralizing the myelin-associated neurite growth inhibitor Nogo-A. *J. Neurosci.* **21,** 3665–3673 (2001).
6. Prinjha, R. *et al.* Inhibitor of neurite outgrowth in humans. *Nature* **403,** 383–384 (2000).
7. Mukhopadhyay, G., Doherty, P., Walsh, F. S., Crocker, P. R. & Filbin, M. T. A novel role for myelin-associated glycoprotein as an inhibitor of axonal regeneration. *Neuron* **13,** 757–767 (1994).
8. McKerracher, L. *et al.* Identification of myelin-associated glycoprotein as a major myelin-derived inhibitor of neurite growth. *Neuron* **13,** 805–811 (1994).
9. Niederost, B. P., Zimmermann, D. R., Schwab, M. E. & Bandtlow, C. E. Bovine CNS myelin contains neurite growth-inhibitory activity associated with chondroitin sulfate proteoglycans. *J. Neurosci.* **19,** 8979–8989 (1999).
10. Weidner, N., Ner, A., Salimi, N. & Tuszynski, M. H. Spontaneous corticospinal axonal plasticity and functional recovery after adult central nervous system injury. *Proc. Natl Acad. Sci. USA* **98,** 3513–3518 (2001).
11. Basso, D. M., Beattie, M. S. & Bresnahan, J. C. A sensitive and reliable locomotor rating scale for open field testing in rats. *J. Neurotrauma* **12,** 1–21 (1995).
12. Takahashi, T., Nakamura, F. & Strittmatter, S. M. Neuronal and non-neuronal collapsin-1 binding sites in developing chick are distinct from other semaphorin binding sites. *J. Neurosci.* **17,** 9183–9193 (1997).
13. Fournier, A. E. *et al.* Semaphorin3A enhances endocytosis at sites of receptor-F-actin colocalization during growth cone collapse. *J. Cell Biol.* **149,** 411–422 (2000).
14. Thallmair, M. *et al.* Neurite growth inhibitors restrict plasticity and functional recovery following corticospinal tract lesions. *Nature Neurosci.* **1,** 124–131 (1998).

Acknowledgements

We thank Y. Fu for technical assistance. This work was supported by grants to S.M.S. from the NIH, the McKnight Foundation for Neuroscience, and Biogen Inc. T.G. is a Bayer Predoctoral Scholar and S.M.S. is an Investigator of the Patrick and Catherine Weldon Donaghue Medical Research Foundation.

Competing interests statement

The authors declare competing financial interests: details accompany the paper on *Nature*'s website (http://www.nature.com).

Correspondence and requests for materials should be addressed to S.M.S. (e-mail: stephen.strittmatter@yale.edu).